

RESEARCH ARTICLE | MAY 01 1991

The spectrum of fractal dimensions of passively convected scalar gradients in chaotic fluid flows

Frank Városi; Thomas M. Antonsen, Jr.; Edward Ott

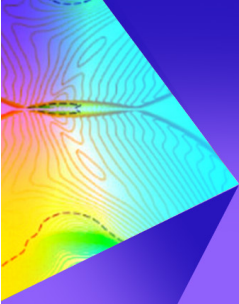


Physics of Fluids A: Fluid Dynamics 3, 1017–1028 (1991)

<https://doi.org/10.1063/1.858081>



CrossMark



Physics of Fluids
Special Topic: Shock Waves
Submit Today!

The spectrum of fractal dimensions of passively convected scalar gradients in chaotic fluid flows

Frank Városi, Thomas M. Antonsen, Jr.,^{a)} and Edward Ott^{a)}
Laboratory for Plasma Research, University of Maryland, College Park, Maryland 20742

(Received 28 August 1990; accepted 20 December 1990)

The passive convection of scalar fields by an incompressible fluid flow in two dimensions is investigated numerically. The prescribed flow is chaotic meaning that nearby fluid elements diverge exponentially with time. The gradient of the convected scalar field is of primary interest, and a measure is defined, reflecting the spatial distribution of the regions having large gradient. The dimension spectrum for this measure is computed by the standard box counting technique, and it is found to be fractal. A recent theory proposes that the fractal structure of the scalar gradient can be related to the nonuniform stretching properties of the flow. Using this theory, the fractal dimension spectrum is computed from the distribution of finite time Lyapunov exponents of the flow, and it is found to be in reasonable agreement with the dimension spectrum computed directly by means of box counting.

I. INTRODUCTION

Suppose a fluid is injected with a small amount of dye or some other kind of contaminant, and this contaminant is convected by the fluid without otherwise influencing the motion of the fluid, thus acting as a passive tracer of the fluid flow. Let $\phi(\mathbf{x}, t)$ be the concentration of the contaminant in the fluid at any position \mathbf{x} and time t . Then the scalar field ϕ satisfies the equation

$$\frac{d\phi}{dt} = \frac{\partial\phi}{\partial t} + \mathbf{v} \cdot \nabla\phi = \xi \nabla^2 \phi, \quad (1)$$

where $\mathbf{v}(\mathbf{x}, t)$ is the fluid velocity field, which we assume to be incompressible, $\nabla \cdot \mathbf{v} = 0$, and ξ is a diffusion coefficient. Thus, the rate of change of the contaminant concentration in a fluid element, while following the flow, is just equal to the diffusion of the contaminant into or out of the fluid element.

In the following, we concentrate on the evolution of the contaminant [Eq. (1)], and we regard the velocity field $\mathbf{v}(\mathbf{x}, t)$ as prescribed, spatially smooth, and possessing spatial structure on large scales only. [In practice $\mathbf{v}(\mathbf{x}, t)$ would be determined by such effects as stirring, thermal convection, etc.] Although $\mathbf{v}(\mathbf{x}, t)$ varies on large scales only, we shall see that the passive scalar field will have variation on very small scales. Initially the diffusion term in Eq. (1) is negligible for small enough ξ . As time proceeds, smaller scale variations of ϕ will develop, until, at some time t_d , diffusion has the effect of smoothing over the gradients in ϕ . We are interested in the relatively short time convection ($t < t_d$) of the passive scalar, and for such cases diffusion can be neglected. The effect of diffusion on the problem we shall consider is discussed in more detail by Ott and Antonsen.^{1,2}

Henceforth we set $\xi = 0$, in which case Eq. (1) reduces to

$$\frac{d\phi}{dt} = 0 \quad (2)$$

so that the concentration ϕ of the passive contaminant in any infinitesimal fluid element is constant as the fluid element is

convected by the flow. Let $\mathbf{x}(t)$ be the position of a fluid element as a function of time. Then the trajectory $\mathbf{x}(t)$ is a solution of

$$\frac{d\mathbf{x}}{dt} = \mathbf{v}(\mathbf{x}, t). \quad (3)$$

Taking an infinitesimal linear variation $\delta\mathbf{x}$ along a trajectory $\mathbf{x}(t)$, one finds $\delta\mathbf{x}(t)$ to satisfy to first order

$$\frac{d\delta\mathbf{x}}{dt} = \delta\mathbf{x} \cdot \nabla\mathbf{v}. \quad (4)$$

In a chaotic flow, typical trajectories have variational solutions $\delta\mathbf{x}(t)$ which are, on average, exponentially increasing in magnitude, so that nearby fluid element trajectories tend to diverge exponentially as time proceeds. Recently, the evolution of contaminants when the fluid element trajectories are chaotic has been the subject of much interest.¹⁻³

Let \mathbf{x}_0 be the initial point of any trajectory and let $\delta\mathbf{x}(0)$ be an initial variation vector. The exponential divergence of nearby trajectories is quantified by a finite time Lyapunov exponent

$$h(t; \mathbf{x}_0) = \frac{1}{t} \ln \frac{|\delta\mathbf{x}(t)|}{|\delta\mathbf{x}(0)|} \quad (5)$$

being positive as the system evolves, for most choices of $\delta\mathbf{x}(0)$. The exact direction chosen for $\delta\mathbf{x}(0)$ is not critical since most initial variation vectors will evolve in the direction of maximal exponential divergence. The quantity $h(t; \mathbf{x}_0)$ indicates the average rate of exponential stretching experienced by a fluid element after having been deformed by the flow for a length of time t . For finite time t this average stretching is typically nonuniform; that is, it depends on the initial position \mathbf{x}_0 . Chaos in a fluid flow is defined more precisely as the existence of a set of initial conditions \mathbf{x}_0 of non-zero volume for which the trajectories $\mathbf{x}(t)$ have asymptotically positive Lyapunov exponents

$$\lim_{t \rightarrow \infty} h(t; \mathbf{x}_0) > 0.$$

Suppose that there is an ergodic region A for the flow.

^{a)} Also at Departments of Physics and Electrical Engineering.

That is, almost any initial condition in A yields a trajectory which eventually comes arbitrarily close to any point in A . In this case, the limit as $t \rightarrow \infty$ of the Lyapunov exponent $h(t; \mathbf{x}_0)$, is the same value, which we denote as \bar{h} , for almost any \mathbf{x}_0 in A . By "almost any" \mathbf{x}_0 we mean that, if we choose \mathbf{x}_0 randomly in the region A , then the probability that $\lim_{t \rightarrow \infty} h(t; \mathbf{x}_0) = \bar{h}$ is one. There is, however, a zero probability (i.e., zero volume) set of \mathbf{x}_0 for which the $t \rightarrow \infty$ limit is not \bar{h} . For finite time, however, we can introduce a distribution,^{2,4} $P(h, t)$, of the finite time Lyapunov exponents, for \mathbf{x}_0 randomly chosen with uniform distribution in the region A . As t increases, $P(h, t)$ becomes more and more sharply peaked at $h = \bar{h}$, approaching a delta function at \bar{h} in the $t \rightarrow \infty$ limit. This distribution will play an important role in our future considerations.

From Eq. (2), the passive scalar field has constant values ϕ_1 and ϕ_2 on two adjacent fluid element trajectories. Thus $\delta\phi = \phi_1 - \phi_2$ is also a constant following the flow. Considering the separation $\delta\mathbf{x}$ between the two trajectories to be infinitesimal, we have $\delta\phi = \delta\mathbf{x} \cdot \nabla\phi$, and therefore

$$\frac{d}{dt} (\delta\mathbf{x} \cdot \nabla\phi) = 0 \quad (6)$$

along any trajectory. In a chaotic flow there are solutions $\delta\mathbf{x}(t)$ which grow exponentially, corresponding to stretching the fluid elements in some direction, but since the flow is incompressible the fluid elements must be shrinking in some other direction. Hence there exist solutions $\delta\mathbf{x}(t)$ of Eq. (4) which decrease exponentially with time causing the magnitude of the scalar gradient, $|\nabla\phi|$, to increase exponentially in order to maintain $\delta\mathbf{x} \cdot \nabla\phi$ constant.

Consider the simple situation of two-dimensional incompressible flow and let $\delta\mathbf{x}_1(t)$ and $\delta\mathbf{x}_2(t)$ be solutions of Eq. (4), chosen so that $|\delta\mathbf{x}_1(t)|$ increases with time and $|\delta\mathbf{x}_2(t)|$ decreases with time. (The more complicated case of three-dimensional field convection is described in Ref. 2.) Using $\hat{\mathbf{z}}$, the unit vector perpendicular to the plane, we can express the scalar gradient in terms of the reciprocal basis

$$\nabla\phi(\mathbf{x}, t) = \alpha_1 (\delta\mathbf{x}_1 \times \hat{\mathbf{z}}) + \alpha_2 (\hat{\mathbf{z}} \times \delta\mathbf{x}_2). \quad (7)$$

We now show that the coefficients α_1 and α_2 are time independent. Consider an arbitrary displacement $\delta\mathbf{x}(t) = \beta_1 \delta\mathbf{x}_1(t) + \beta_2 \delta\mathbf{x}_2(t)$ and compute

$$\delta\phi = \delta\mathbf{x}(t) \cdot \nabla\phi(\mathbf{x}, t) = \delta V(\beta_1 \alpha_2 + \beta_2 \alpha_1),$$

where

$$\delta V = \delta\mathbf{x}_1 \cdot (\hat{\mathbf{z}} \times \delta\mathbf{x}_2) = \delta\mathbf{x}_2 \cdot (\delta\mathbf{x}_1 \times \hat{\mathbf{z}})$$

is the area of the parallelogram formed by $\delta\mathbf{x}_1$ and $\delta\mathbf{x}_2$, and since the flow is incompressible, δV is constant. Since $\delta\phi$ is constant due to Eq. (6), and the coefficients β_k are arbitrary constants, we conclude that the coefficients α_k must be constant. If $\delta\mathbf{x}_1(t)$ grows exponentially and $\delta\mathbf{x}_2(t)$ decreases exponentially, we have

$$|\nabla\phi(\mathbf{x}, t)| \sim |\delta\mathbf{x}_1(t)| \sim e^{h(t; \mathbf{x}_0)t} \quad (8)$$

from Eq. (7). Thus $\nabla\phi$ grows exponentially in a direction orthogonal to $\delta\mathbf{x}_1(t)$. Further, for large t , due to the dependence of the finite time exponent $h(t; \mathbf{x}_0)$ on initial condition, there will be large variations in the gradient from point to

point in the fluid. Small regions with particularly large values of h will appear as "hot spots."

Based on the preceding discussion, in a typical chaotic flow with a nonuniform distribution of stretching rates, it has been shown^{1,2} that $\nabla\phi$ will tend to concentrate on a fractal set, after long enough time, and that the spectrum of spatial scaling exponents (defined subsequently) of the fractal properties of $\nabla\phi$ is directly related to the distribution of exponential stretching rates (finite time Lyapunov exponents). With this in mind, define a time evolving measure μ_ϕ of any subset S of the ergodic region A occupied by the fluid:

$$\mu_\phi(S, t; \gamma) = \frac{\int_S |\nabla\phi|^\gamma dV}{\int_A |\nabla\phi|^\gamma dV}. \quad (9)$$

Ott and Antonsen² have formulated equations which allow computation of the dimension spectrum of μ_ϕ in terms of the distribution of Lyapunov exponents. The goal of this paper is to numerically verify the theory² for a two-dimensional flow. We note that the fractal dimensions of such a measure (with $\gamma = 2$) has been measured experimentally,⁵ both for a turbulent flow and for a smooth, presumably chaotic flow (as considered in our paper).

In Sec. II a particular two-dimensional chaotic flow is introduced, and the passive convection of an initial scalar field and its gradient is computed. Images of the scalar gradient measure (9) are shown as a function of time and these images clearly illustrate that the gradient measure asymptotes to a multifractal. In Sec. III we compute the dimension spectrum of the measure directly from the images using box counting, and compare it with the spectrum of dimensions obtained from the distribution of Lyapunov exponents. Section IV is a review of the theory relating the dimension spectrum of a scalar gradient measure to the Lyapunov exponent distribution for the fluid flow. Section V then explains how this theory is applied, using the numerically determined distribution of stretching rates in the two-dimensional chaotic flow to calculate the dimension spectrum. The comparison with the box counting dimension spectra is then examined in more detail. Section VI gives a summary with conclusions, and, in the Appendix we discuss the equivalence of the problem we treat to that of the evolution of an initially smooth line or surface convected with the flow.

II. IMAGES OF THE SCALAR FIELD AND GRADIENT

In our numerical studies we choose to solve Eqs. (3) and (4) for a particular choice of flow $\mathbf{v}(\mathbf{x}, t)$ which leads to a discrete time mapping for the trajectory equations. In general, a mapping can be derived from a continuous time flow by the following arguments. Given a flow velocity field $\mathbf{v}(\mathbf{x}, t)$ one can integrate Eq. (3) over a time interval T from nT to $(n+1)T$, where $n = 0, 1, 2, \dots$, and obtain a mapping

$$\mathbf{x}_{n+1} = \mathbf{M}(\mathbf{x}_n, n) \quad (10)$$

giving discrete positions \mathbf{x}_n along a fluid trajectory, which is then also called an orbit of the map. The mapping will depend explicitly on the time step n if the flow is not periodic with period T , and, in particular, if there is nonperiodic time dependence in the velocity field. The theory of Refs. 1 and 2

applies to both the cases of periodic and nonperiodic time dependence of the Eulerian velocity $\mathbf{v}(\mathbf{x},t)$. The particular numerical example reported in detail in this paper will involve a map \mathbf{M} that depends explicitly on n and is meant to model a flow with complicated time dependence. We also briefly discuss at the end of Sec. II and the end of Sec. IV, numerical results for the time periodic case where \mathbf{M} is independent of n .

The discrete time evolution of an infinitesimal variation following an orbit is then given as a linear mapping

$$\delta\mathbf{x}(n+1) = \mathbf{J}(\mathbf{x}_n, n) \cdot \delta\mathbf{x}(n) \quad (11)$$

[corresponding to Eq. (4)], where $\mathbf{J} = \nabla\mathbf{M}$ is the Jacobian matrix of partial derivatives with respect to \mathbf{x}_n of the mapping \mathbf{M} . We shall use Eq. (11) along with Eq. (7) to compute the discrete time evolution of $\nabla\phi$ for an initial nonuniform scalar field $\phi_0(\mathbf{x})$ specified at $t = 0$.

Specifically, we consider the following spatially smooth velocity field $\mathbf{v}(\mathbf{x},t)$ in our two-dimensional computations, with $\mathbf{x} = (x,y)$:

$$\mathbf{v}(\mathbf{x},t) = v_1 y \hat{\mathbf{x}} + v_2 \sin[\phi(t) + x] \delta_T(t) \hat{\mathbf{y}}, \quad (12)$$

where $\delta_T(t) = T \sum_{n=0}^{\infty} \delta(t - nT)$ is a periodic impulse function, and $\hat{\mathbf{x}}$ and $\hat{\mathbf{y}}$ are unit vectors in the x and y directions. The time dependence of $\theta(t)$ is not periodic, and so the map \mathbf{M} will depend on n [e.g., if $\theta(nT)$ is a constant, the velocity field would then give an exactly periodic flow]. The first term in (12) represents a uniform shear in the x velocity, while the second term is a time- and space-dependent shear in the y velocity of the fluid flow, applied impulsively every time step. A prime motivation for the choice (12) is, of course, that it allows an analytical derivation of a map. The delta function time dependence, while not present in physical flows, is expected to lead to a map which will exhibit behavior of maps that are obtained from typical physical flows.

Integration of Eq. (12) through one forcing period $T = 2\pi$ gives the following mapping of points $\mathbf{x}_n = (x_n, y_n)$ along a trajectory:

$$\begin{aligned} x_{n+1} &= x_n + y_n, \\ y_{n+1} &= y_n + K \sin(x_{n+1} + \theta_n), \end{aligned} \quad (13)$$

with $K = v_1 v_2 T$, and where θ_n are the discrete values of $\theta(t = nT)$. Note that the map (13) is spatially periodic, with period 2π in both x and y . Thus, if the initial distribution of the passive scalar $\phi(\mathbf{x},0)$ is also periodic with periodicity length 2π in x and y , then it remains so for all subsequent time. In such a case, points (x,y) and $(x \pm 2k\pi, y \pm 2m\pi)$ are equivalent, and thus we can take (x_n, y_n) modulo 2π in our computations. With $\theta_n \equiv 0$, Eq. (13) is the familiar standard map (or kicked rotor map), which is known to have a mixture of chaotic orbits and invariant KAM curves surrounding stable periodic orbits.

In this paper we shall take the point of view that $\theta(t)$ is complicated function of time (possibly having chaotic Eulerian time dependence). Our results obtained with this choice of $\theta(t)$ are expected to be a good qualitative indication of behavior in general flows with complex time dependence of the velocity field $\mathbf{v}(\mathbf{x},t)$. Thus we shall assume θ_n to

be random and uncorrelated at each time step n . With this prescription for θ_n , there can be no KAM surfaces or periodic orbits, and orbits are ergodic in the entire square $0 \leq (x,y) < 2\pi$. Furthermore, for any $K > 0$ orbits with nearby initial conditions typically diverge exponentially. For definiteness, we take the distribution of θ_n to be uniform in $(0, 2\pi)$. We emphasize that, although the map (13) and our prescription for θ_n follow from a specific realization of $\mathbf{v}(\mathbf{x},t)$, we expect that the behavior found is typical of a broad class of flows.

The Jacobian of the randomized standard map $\mathbf{M}(\mathbf{x}_n, \theta_n)$ in Eq. (13) is

$$\begin{aligned} \mathbf{J}(\mathbf{x}_n, \theta_n) &= \begin{bmatrix} 1 & 1 \\ K \cos(x_{n+1} + \theta_n) & 1 + K \cos(x_{n+1} + \theta_n) \end{bmatrix}. \end{aligned} \quad (14)$$

Note the explicit dependence of \mathbf{M} and \mathbf{J} on the random sequence θ_n , so that both the flow trajectories and the deformation of fluid elements have random components. Using the value $K = 0.5$ in the randomized standard map, and numerically computing the Lyapunov exponent (5) via Eq. (11), we find that $\lim_{t \rightarrow \infty} h(t; \mathbf{x}_0) = \bar{h} \approx 0.143$ for all initial conditions \mathbf{x}_0 tested.

In order to obtain images of the convected scalar field and its gradient, we shall compute these quantities on an equally spaced grid. To do this we start at a grid point and iterate backwards in time to find the initial points, which, upon forward iteration would arrive at the original grid point (supposing an ideal computer). This forward iteration is not performed: all that is needed is to save the trajectories already computed from the inverse map, and apply the Jacobian mapping, Eq. (11), in forward time to obtain the variations $\delta\mathbf{x}(n)$, which then give $\nabla\phi$ using Eq. (7).

The computational scheme is as follows. A sequence of uniformly distributed random numbers $0 < \Psi_n < 2\pi$ is chosen for the computation of the θ_n values. Suppose the value of the convected field at grid point \mathbf{x}_g and time $t = NT$ is required. The trajectory which ends at \mathbf{x}_g is obtained by applying the inverse of the mapping (13) to the point $\mathbf{x}_N = \mathbf{x}_g$ for $n = N, N-1, N-2, \dots, 1$ iterations,

$$\mathbf{x}_{n-1} = \mathbf{M}^{-1}(\mathbf{x}_n, \theta_n), \quad (15)$$

with $\theta_n = \Psi_{N-n}$, to arrive at the initial point, \mathbf{x}_0 , of the trajectory. Since ϕ is constant along trajectories [Eq. (2)] we have simply

$$\phi(\mathbf{x}_n, nT) = \phi_0(\mathbf{x}_0),$$

where ϕ_0 is the initial scalar field, and for $n = N$ this yields the desired value at the grid point. Substituting $N+1$ for N in the preceding scheme shows that computation of an image at time $t = (N+1)T$ is accomplished by adding one more inverse iteration to the already computed trajectories. Furthermore, choosing $\theta_n = \Psi_{N+1-n}$ causes trajectories making up the image of the convected field at time $(N+1)T$ to share the same final history for the random sequence θ_n as trajectories in the image at time NT , or at any other time. Thus, the final time steps of the flow always follow the same pattern given by the elements of the random sequence $\Psi_1, \dots, \Psi_3, \Psi_2, \Psi_1, \Psi_0$, no matter how many time steps are

computed. We shall discuss the reason for this choice subsequently.

In the following computations the initial scalar field used is $\phi_0(\mathbf{x}) = \sin x$ where $\mathbf{x} = (x, y)$, giving $\nabla\phi_0(\mathbf{x}) = (\cos x, 0)$. Then using the reciprocal basis representation of Eq. (7) and choosing

$$\delta\mathbf{x}_1(0) = (0, \cos x), \quad \delta\mathbf{x}_2(0) = (1, 0)$$

for the initial linear displacements, gives $\alpha_1 = 1$ and $\alpha_2 = 0$ in Eq. (7). The evolution of the variation $\delta\mathbf{x}_1(n)$, $n = 0, 1, 2, \dots, N$ is then computed as

$$\delta\mathbf{x}_1(n+1) = \mathbf{J}(\mathbf{x}_n, \theta_n) \cdot \delta\mathbf{x}_1(n) \quad (16)$$

using the Jacobian of the map, where $\theta_n = \Psi_{N-n}$. We then have $|\nabla\phi(\mathbf{x}_n, nT)| = |\delta\mathbf{x}_1(n)|$, and $\nabla\phi$ is orthogonal to $\delta\mathbf{x}_1$.

In Fig. 1 are shown computed images of the scalar field (on the left side) and the magnitude of the gradient (on the right side), at increasing iterations n of the randomized standard map with $K = 0.5$. The scalar field and its gradient are computed on a uniform grid of 768×768 points, and images of the scalar field ϕ and $|\nabla\phi|$ are obtained by averaging over 2×2 groups of points, thereby yielding images of 384×384 pixels.

A linear intensity scale is used for the images of the scalar field ϕ : pixels with $-1 < \phi < 0$ are in shades of dark blue to violet, while pixels with $0 < \phi < 1$ are in shades of red to yellow. As time progresses, the images of ϕ get more com-

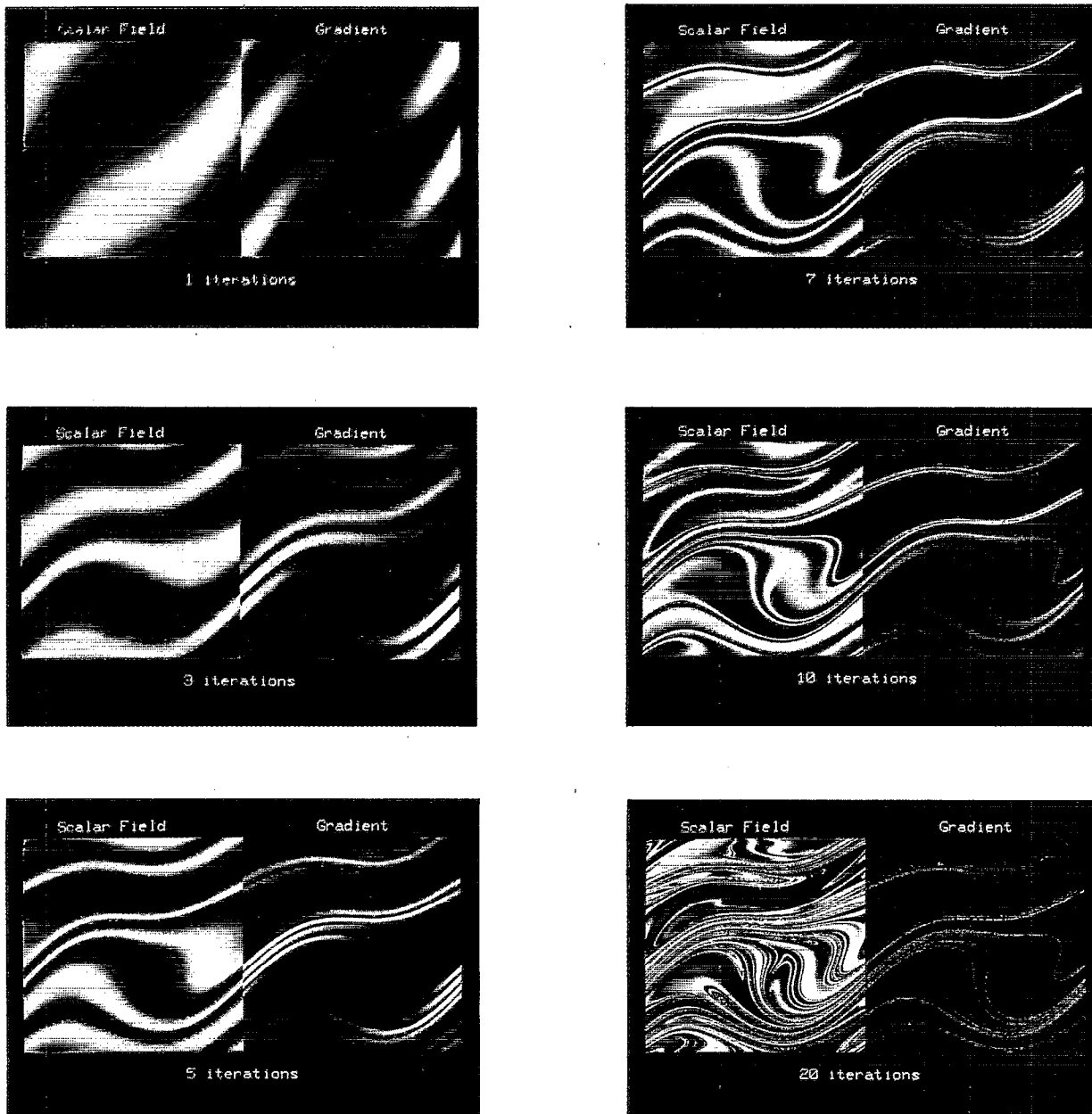


FIG. 1. Images of the passively convected scalar field (left side) and the magnitude of its gradient (right side), where the two-dimensional chaotic flow is given by the randomized standard map, Eq. (13) with $K = 0.5$. The iterations shown are $n = 1, 3, 5, 7, 10, 20$. The coloring is explained in the text.

plicated, but maintain the same range of magnitudes. For any value C , the area of the region where $\phi > C$ remains constant for all time. Thus, $|\phi|$ does not concentrate on a fractal.

On the other hand, since $|\nabla\phi|$ grows at widely varying exponential rates, a linear intensity scale is not appropriate for the display of the $|\nabla\phi|$ images because only a few points would be visible. Therefore the images of $|\nabla\phi|$, displayed in the right halves of the panels in Fig. 1, are scaled in the following manner. The image intensity at a particular pixel P is obtained by computing

$$\mathcal{F}(P) = \sum_{\{X\}_P} |\nabla\phi(X)| \left(\sum_{\{Y\}} |\nabla\phi(Y)| \right)^{-1}, \quad (17)$$

where $\{X\}_P$ denotes those pixels for which $|\nabla\phi(X)| < |\nabla\phi(P)|$, and $\{Y\}$ denotes all pixels. The relation between $\mathcal{F}(P)$ and the measure $\mu_\phi(P)$ defined in Eq. (9) with $\gamma = 1$, is as follows: the intensity $\mathcal{F}(P)$ is equal to the *measure* of the pixels which individually all have $|\nabla\phi|$ less than $|\nabla\phi(P)|$. [Thus, for example, the region where $\mathcal{F}(P) > 0.5$ is the smallest region containing 50% of the total μ_ϕ measure.] The coloring of the images is then determined by $\mathcal{F}(P)$: pixels with $0.1 < \mathcal{F}(P) < 0.5$ are in shades of blue to violet, whereas shades of red to yellow represent pixels with $0.5 < \mathcal{F}(P) < 1$.

By following the red and yellow colored pixels in the images of $|\nabla\phi|$ as time advances, it is clearly seen that 50% of the total measure becomes concentrated in a very small area. The set of all nonblack pixels (blue, violet, red, and yellow) contain 90% of the total measure, illustrating that most of the gradient measure tends to concentrate in an area which decreases with time. In addition, successive iterations of the mapping create more layers of structure in the images, at finer and finer scales. For example, comparison in Fig. 1 of $n = 3$ and $n = 5$ iterations reveals that each bright banded striation at early times is replaced at later time by several thinner striations. Further, the later time thinner striations occupy the same region as the earlier thicker striations. As time progresses, this process repeats. This behavior characterizes the development of a Cantor set of striations. Together, these characteristics indicate the development of a multifractal measure of the gradient as the scalar field is convected by the flow.

The almost stationary appearance of the large scale features in the images of ϕ and $|\nabla\phi|$ shown in Fig. 1 is a consequence of choosing $\theta_n = \Psi_{N-n}$ in Eqs. (15) and (16). Formation of the fractal structure results from iterations of the chaotic map, but the large scale organization is due to the final few iterations of the mapping, and is influenced by the random sequence θ_n . In our computations, the final iterations use the same values of θ_n , no matter how many total iterations are performed. As the total number of iterations is increased from the first image to the next ones, new random numbers θ_n are added only at the beginning of trajectories. If instead, new random numbers were added at the end of trajectories, the multifractal structure of the measure would still develop, but the images from one time step to the next would have a completely different large scale appearance. Presumably (as implied by the analysis of Refs. 1 and 2), quantities such as the dimension spectrum (discussed in the

next section) which characterize the fractal properties of the measure (9), are unaffected by such temporal fluctuations in the large scale pattern (this is corroborated by numerical simulations). Thus these quantities are of fundamental interest.

When there is no random component of the mapping (i.e., $\theta_n \equiv 0$), the large scale features of $|\nabla\phi|$ become stationary as n increases. Examining images (not shown) of the magnitude of the gradient computed when $\theta_n \equiv 0$ and $K = 1$ in the standard map, we observe that the fractal structure of $|\nabla\phi|$ is interspersed with areas of nonfractal structure resulting from invariant KAM curves.

III. DIMENSION SPECTRUM FROM BOX COUNTING

The concept of a multifractal measure is quantified by the following definition of the spectrum of fractal dimensions of a measure. Divide the space occupied by the fluid into a grid of square boxes of size ϵ , and let μ_i be the measure in box i . Then, using boxes of decreasing size $\epsilon \rightarrow 0$, we have the definition of the spectrum of Rényi⁶ dimensions for a measure:

$$D_q = \frac{1}{q-1} \lim_{\epsilon \rightarrow 0} \frac{\log \sum_i \mu_i^q}{\log \epsilon}, \quad (18)$$

where $-\infty < q < +\infty$ is an index. This definition was introduced in the context of natural measures occurring in dynamical systems, by Grassberger,⁷ and Hentschel and Procaccia.⁸ The case of $q = 0$ reduces to the box counting dimension

$$D_0 = \lim_{\epsilon \rightarrow 0} \frac{\log N(\epsilon)}{\log (1/\epsilon)},$$

where $N(\epsilon)$ is the number of boxes having positive measure. The special case of $q = 1$ requires taking the limit $q \rightarrow 1$ in Eq. (18), and gives

$$D_1 = \lim_{\epsilon \rightarrow 0} \frac{\sum_i \mu_i \log \mu_i}{\log \epsilon},$$

which is called the information dimension.⁹ It can be shown from Eq. (18) that D_q is a nonincreasing function of q . The word multifractal is used to describe situations in which D_q varies (decreases) with increasing q .

In applying the definition (18), we examine the measure μ_ϕ of Eq. (9) at finite times n , and, on a sufficiently small scale it is found to be smooth (nonfractal). However, as time increases the scale size at which the measure is smooth, becomes smaller. Hence for our problem define

$$D_q = \frac{1}{q-1} \lim_{\epsilon \rightarrow 0} \lim_{n \rightarrow \infty} \frac{\log \sum_i \mu_i^q}{\log \epsilon}. \quad (19)$$

Estimates of the spectrum of dimensions, $D(q, n)$, are then obtained (cf. below) by observing the scaling of the measure over a finite range of box sizes ϵ , at increasing time. For large enough n we expect $D(q, n) \approx D_q$, and, in Sec. V we determine, for a given range of ϵ , the values of n at which agreement is expected.

When analyzing an image, the box of minimum size is a pixel, and the box sizes are naturally increased by factors of 2, so it is convenient to define the box sizes as $\epsilon_k = 2^{-k}$, for $0 < k < k_p$, where $\epsilon_p = 2^{-k_p}$ is the size of a pixel. The coarse grained measure $\mu_j(\epsilon_k, n)$ in box j of size $\epsilon_k = 2^{-k}$ after n

iterations is simply computed as the sum of the measures in four boxes of the next smaller size, $\epsilon_{k+1} = 2^{-k-1}$, which are in the box j . Applying this relation recursively defines the coarse grained measures for all box sizes in terms of the computed measure of the pixels in the image. Now, for all box sizes, and selected values of q and n , compute the following quantity

$$I_q(\epsilon_k, n) = \frac{1}{q-1} \log_2 \sum_j \mu_j(\epsilon_k, n)^q, \quad (20)$$

and for the case $q = 1$

$$I_1(\epsilon_k, n) = \sum_j \mu_j \log_2 \mu_j.$$

We take I_q to be of the form [cf. Eq. (18)]

$$I_q(\epsilon_k, n) \approx D(q, n) \log_2 \epsilon_k + C(q, n), \quad (21)$$

for $\epsilon_k \ll 1$ and large enough n . To estimate the value of $D(q, n)$, the standard procedure is to use the slope of a linear least-squares fit to I_q vs $\log_2 \epsilon_k$, over some restricted range of box sizes $\epsilon_{\min} < \epsilon_k < \epsilon_{\max}$.

Following the scheme described by Eqs. (15) and (16), the gradient of the scalar field is computed on a grid of 2048×2048 points, for $n = 40$ iterations, and Eq. (9) with $\gamma = 1$, directly gives a 2048×2048 pixel image of the gradient measure μ_ϕ . Box counting analysis is performed on this image by coarse graining the measure and applying Eq. (20), as described above. Figure 2 shows the resulting $I_q(\epsilon, n)$ vs $\log_2 \epsilon$ for values of $0 < q < 1$ and $n = 40$, and for $q > 0$, the graphs exhibit approximately linear behavior over only a limited range of box sizes: $-6 < \log_2 \epsilon < -3$. For this box size range, $D(q, n)$ is estimated by linear least-squares fits to $I_q(\epsilon, n)$, using the form (21). Figure 3 shows the estimated $D(q, n)$, as diamond symbols, with error bars giving

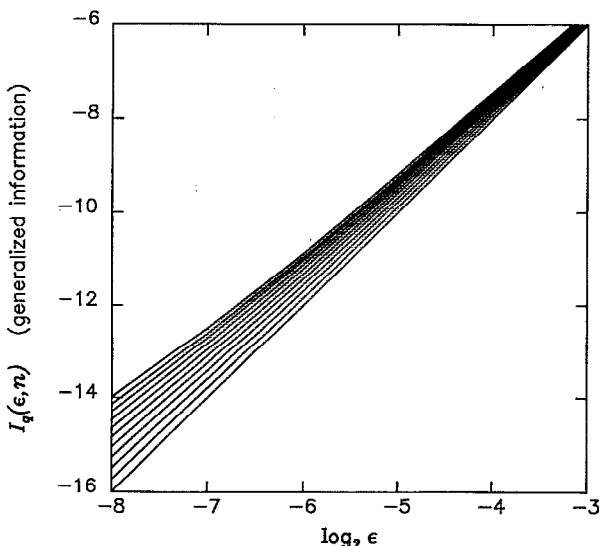


FIG. 2. Results from box counting analysis of a computed image of the gradient measure, μ_ϕ of Eq. (9) with $\gamma = 1$, after $n = 40$ time steps of the flow (iterations of the map with $K = 0.5$). The gradient of the scalar field was computed on a grid of 2048 by 2048 points ($\approx 4\,000\,000$ points). The graph shows $I_q(\epsilon, n)$ [cf. Eq. (20)] versus $\log_2 \epsilon$ ($\epsilon =$ box size), for 11 equally spaced values of q between 0 and 1. The lowest curve in the figure is for $q = 0$ and the highest is for $q = 1$.

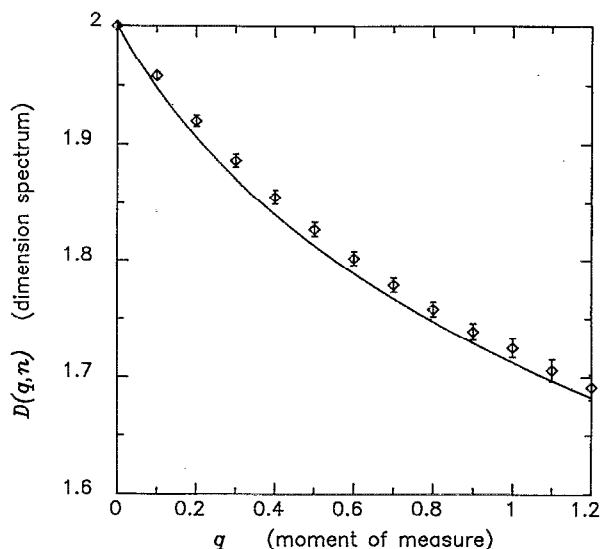


FIG. 3. The diamond symbols with error bars show the box counting dimension spectrum $D(q, n = 40)$ estimated by linear least-squares fits to $I_q(\epsilon, n)$ of Fig. 2 over the box size range $2^{-6} \leq \epsilon < 2^{-3}$. The error bars indicate the standard deviation of the errors between the data and each fit. The solid curve is the dimension spectrum obtained from the distribution of Lyapunov exponents, as explained in Sec. V.

the root mean square of deviations between the linear fits and the I_q data. We find that the error bars indicate the approximate deviations from linearity in the I_q vs $\log_2 \epsilon$ graphs, over the range fitted. In our computations of the convected scalar gradient, all boxes always have some positive measure so it is always the case that $D_0 = 2$, and thus the error bars tend to zero as $q \rightarrow 0$.

The solid curve in Fig. 3 is the dimension spectrum predicted from the distribution of Lyapunov exponents at $n = 100$. We note that this dimension spectrum is relatively constant for $n > 50$ because it is based on a time invariant characteristic of the Lyapunov exponent distribution, as explained in Sec. VI and demonstrated in Sec. V. The box counting dimension spectrum for $n = 40$ agrees reasonably well with this theory, when estimated using a small range of box sizes, $-6 < \log_2 \epsilon < -3$, as shown in Fig. 3. If the $I_q(\epsilon, n)$ data in Fig. 2 for $\log_2 \epsilon < -6$ are included in the least-squares fitting, the resulting estimates of $D(q, n)$ for $q > 0.6$ are found (not shown here) to drop below the dimension spectrum predicted from the Lyapunov exponent distribution and they have much larger error bars. The basic limit on the observable scaling range of the measure is determined by the number of points per box at which the scalar field gradient is computed. For $\log_2 \epsilon = -6$ this is $(2048)^2 \times (2^{-6})^2 = 1024$, but for $\log_2 \epsilon = -7$ there are only 256 points per box, which is found to be too few for accurate estimation of the gradient measure in two-dimensional boxes, when $n = 40$.

The range of box sizes useful for estimating $D(q, n)$, for large n , is quite limited when analyzing an image, because, for a fixed number of points, the uncertainty in estimating the gradient measure of two-dimensional boxes grows quadratically as the box size is decreased. In addition, the storage and computation time required increases quadratically

with decreasing box size, since the scalar gradient must be computed at some minimum number of points per box. Therefore, to reduce uncertainties of the box counting analysis, we also compute μ_ϕ on a randomly chosen vertical line through the image. Since the boxes are then intervals, computing the scalar gradient at the same number of points (2048^2) enables the use of much smaller box sizes, while still having many points per box. We calculate I_q as before and obtain an estimate $\bar{D}(q,n)$ for the fractal dimension of the intersection of the measure with the line. The striated structure seen in Fig. 1 implies that the measure is smoothly varying in one direction (i.e., along the striations), and thus $D(q,n) = 1 + \bar{D}(q,n)$. The preceding assumes that the randomly chosen line is nowhere tangent to the striations. We assume that if tangencies of the fractal striations with the line do occur, they are infrequent enough not to affect the value of D_q for q in the range of interest ($0 < q < 1$). Indeed, the following results seem to bear this out.

The resulting I_q and $D(q,n)$ for a vertical cut through the fluid flow are shown in Figs. 4(a) and 4(b), respectively. The range of box sizes for which I_q scales logarithmically has greatly increased, and using box sizes in the range $2^{-13} < \epsilon < 2^{-3}$ results in the estimates of $D(q,n)$ shown in Fig. 4(b) (diamonds with error bars). The box counting dimension now agrees better with the prediction based on Lyapunov exponents (the solid curve), and the estimated dimension spectrum is more robust and convincing, since it is based on a larger scaling range than what was obtainable from analyzing an image. Using a slightly smaller range of box sizes does not significantly affect the estimates of $D(q,n)$. We conclude that the error bars are due to statistical fluctuations of I_q over the scaling range. Performing the box counting analysis for a few other randomly chosen lines intersecting the gradient measure results in I_q vs $\log_2 \epsilon$ graphs having different fluctuations, but the resulting estimates of $D(q,n)$ are within the error bars of Fig. 4(b).

Figures 2–4 were at fixed values of time n . To estimate the limiting dimension spectrum, we show in Fig. 5 the box counting dimension spectrum, $D(q,n)$, as a function of iterations n , for the particular values of $q = 0.5$ and $q = 1$. The diamond symbols with error bars are $D(q,n)$ estimated using the box size range $2^{-13} < \epsilon < 2^{-3}$. The solid horizontal lines are the dimensions for $q = 0.5$ and $q = 1$, calculated from the distribution of Lyapunov exponents at $n = 100$. For each value of q , there is a range of n in which the variation of $D(q,n)$ with n is almost constant and the error bars are smallest: $30 < n < 60$ for $q = 1$, and $50 < n < 80$ for $q = 0.5$. For these ranges of n , there exists numerically observed multifractal scaling of the gradient measure, and the box counting dimension estimates are in agreement with the Lyapunov dimensions.

The following is a heuristic explanation of the observed behavior of $D(q,n)$ as a function of iterations n , when estimated using a fixed range of box sizes and a uniform grid of points. As the number of iterations increases, the multifractal scaling of the measure is created by the chaotic flow, and the values of $D(q,n)$ decrease from 2 toward the values predicted by the theory, as seen in Fig. 5. However, after some number iterations, depending on q , the box counting dimen-

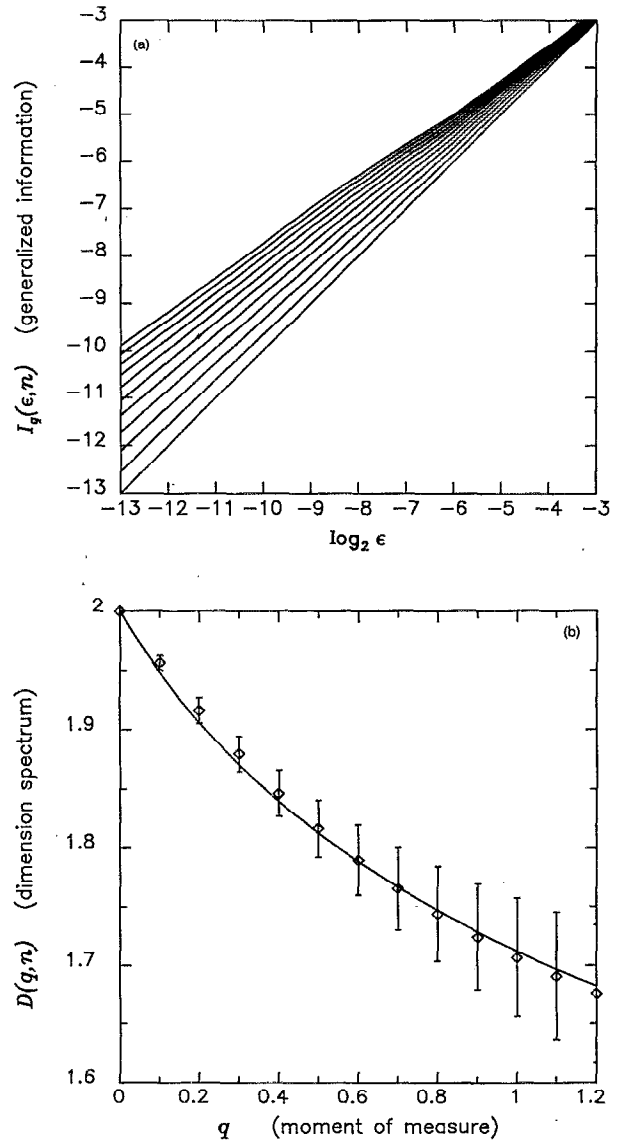


FIG. 4. In this case, the gradient measure was computed at 4 000 000 points along a vertical line intersecting the flow at $x = 3.2778$, where x was chosen at random. The box counting results at time $n = 50$ are shown in: (a) $I_q(\epsilon, n)$ vs $\log_2 \epsilon$ for $0 < q < 1$, (b) diamonds with error bars show $D(q, n) = 1 + \bar{D}(q, n)$, where $\bar{D}(q, n)$ is obtained from linear least-squares fits to I_q of (a), over the range $2^{-13} < \epsilon < 2^{-3}$, and the solid curve is the Lyapunov dimension spectrum.

sion estimates $D(q,n)$ decrease below the predictions based on the Lyapunov exponent distribution. This occurs because for large n there is an insufficient number of pixels for obtaining good statistical estimates. This behavior of $D(q,n)$ as a function of both q and n is explained in more detail in Sec. V using the distribution of Lyapunov exponents.

IV. SPECTRUM OF DIMENSIONS AND THE DISTRIBUTION OF LYAPUNOV EXPONENTS

In this section we review the theory relating the dimension spectrum D_q of the measure μ_ϕ of a convected scalar to

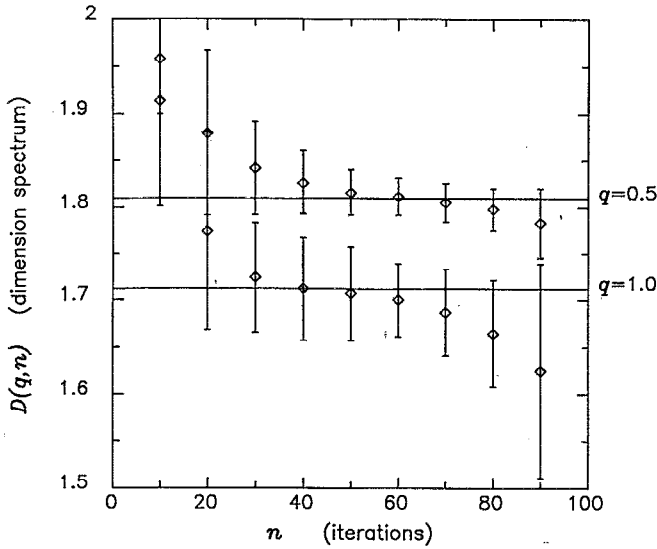


FIG. 5. Analyzing the same vertical cut discussed in Fig. 4, this time we show $D(q, n) = 1 + \bar{D}(q, n)$ (diamonds with error bars) for particular values of $q = 0.5$ and $q = 1$, while varying $0 < n < 100$. Again, $\bar{D}(q, n)$ is obtained from linear least-squares fits to $I_q(\epsilon, n)$ over the range $2^{-13} < \epsilon < 2^{-3}$. The solid horizontal lines are the corresponding dimensions obtained from the distribution of Lyapunov exponents.

the distribution of stretching rates in the flow. The connection is accomplished with a partition function approach. To describe natural measures which occur in dynamical systems, Grassberger¹⁰ and Halsey *et al.*¹¹ introduced a partition function which combines the general properties of the definition of Hausdorff dimension (purely geometric) with the definition (18) of Rényi dimensions of a measure.

In order to describe passive convection by a flow, Ott and Antonsen^{1,2} have combined the partition function formulation with the knowledge of how the magnitude of the scalar gradient grows in a chaotic flow to define a new partition function based on the stretching properties of the flow. Considering the flow as a mapping using Eqs. (10) and (11), define the stretching along a fluid trajectory starting at \mathbf{x}_0 after n iterations as

$$L(n; \mathbf{x}_0) = \frac{|\delta \mathbf{x}(n)|}{|\delta \mathbf{x}(0)|}, \quad (22)$$

where $\delta \mathbf{x}(0)$ is an initial infinitesimal variation at \mathbf{x}_0 , chosen in a direction which causes the above quantity L to increase. Note that

$$L(n; \mathbf{x}_0) = \exp[nh(n; \mathbf{x}_0)],$$

where h is the finite time Lyapunov exponent of Eq. (5), and we have set the mapping time step $T = 1$ for convenience. Recall from Eqs. (7) and (8) that $|\nabla \phi| \sim L$ in a two-dimensional incompressible flow. Using this fact in the definition (9) of the time evolving gradient measure $\mu_\phi(\cdot, n; \gamma)$ and utilizing the partition function formulation of Rényi dimensions, the following Lyapunov partition function can be derived^{1,2}

$$\Gamma(n, q, D) \equiv \langle L^{\sigma(q)} \rangle / \langle L^\gamma \rangle^q, \quad (23)$$

with

$$\sigma(q) \equiv (q - 1)(D - 2) + \gamma q,$$

and where $L = L(n; \mathbf{x}_0)$ and the angle brackets denote an average over initial conditions \mathbf{x}_0 uniform in the ergodic region. For $n \rightarrow \infty$ the quantity $\Gamma(n, q, D)$ will approach infinity if $(q - 1)D$ is larger than a critical value τ_q , while it will approach zero if $(q - 1)D$ is smaller than τ_q . For a particular value of q , the spectrum index, the dimension D_q of the measure as $n \rightarrow \infty$ is then given by the critical value of D at which the quantity

$$\Gamma(q, D) = \lim_{n \rightarrow \infty} \Gamma(n, q, D) \quad (24)$$

goes from zero to infinity as $(q - 1)D$ increases; i.e., $D_q = \tau_q / (q - 1)$.

The partition function (23) demonstrates the intimate connection between the distribution of finite time Lyapunov exponents h (or equivalently L) and the spectrum of dimensions D_q . Further, it is necessary that there be a distribution of exponents $h(n; \mathbf{x}_0)$ for the measure to be multifractal: In the trivial case where all initial conditions \mathbf{x}_0 yield the same $h(n; \mathbf{x}_0)$, Eqs. (23) and (24) yield D_q independent of q and equal to 2.

Recall from the Introduction that we denote the distribution of finite time Lyapunov exponents by $P(h, n)$, and when the number of iterations n is large,

$$\bar{h} \cong \int_0^\infty P(h, n) h \, dh,$$

where $\bar{h} = \lim_{n \rightarrow \infty} h(n; \mathbf{x}_0)$ is the common value of the limit assumed by almost any choice of \mathbf{x}_0 . For a particular solvable model (the generalized baker's map), the distribution of Lyapunov exponents has been shown^{2,9} to be of the form

$$P(h, n) = [nG''(h)/2\pi]^{1/2} \exp[-nG(h)] \quad (25)$$

for large n . In addition, (25) has been argued on general grounds to apply^{4,12} for dissipative two-dimensional maps such as the Hénon map. The distribution (25) becomes peaked at \bar{h} , with a width that decreases as $n^{-1/2}$, and so at \bar{h} the function G must reach its minimum value ($G'(\bar{h}) = 0$) and the normalization condition requires that $G(\bar{h}) = 0$. In the case of time periodic two-dimensional incompressible flows there can be significant deviations from (25) because of the stickiness of the KAM curves bounding the relevant ergodic region.^{13,14} However, this does not apply for our study by virtue of the choice of a nonperiodic $\theta(t)$ in Eq. (12) and the consequent absence of KAM invariant curves.

For cases where the above form (25) of the Lyapunov exponent distribution applies (e.g., temporally chaotic fluid flows), we can use this representation to compute the p -order moment of L by the method of steepest descent

$$\langle L^p \rangle = \int_0^\infty P(h, n) e^{pn h} \, dh \sim \exp\{-n[G(h_p) - p h_p]\}, \quad (26)$$

where h_p is determined by the saddle point condition

$$\left. \frac{dG}{dh} \right|_{h=h_p} = p. \quad (27)$$

Note that the range Δh_p , around h_p , which gives the main contribution to the integral (26) is

$$\Delta h_p \sim \sqrt{2/nG''(h_p)}. \quad (28)$$

Using the result (26) in the partition function (23) gives the following condition for $\Gamma(n, q, D)$ to be finite and nonzero as $n \rightarrow \infty$:

$$G(h_\sigma) - \sigma h_\sigma = q[G(h_\gamma) - \gamma h_\gamma]. \quad (29)$$

The above condition determines the critical value of $\sigma(q)$ in the partition function, which then yields

$$D_q = 2 - [\gamma q - \sigma(q)] / (q - 1). \quad (30)$$

Thus the dimension spectrum of μ_ϕ in a two-dimensional flow is completely determined by the function $G(h)$.

We now show that the values of h_σ and h_γ will both be greater than \bar{h} for $q > 0$ and $\gamma > 0$. We note from (23) that the critical value of σ at which $\Gamma(q, D)$ has its transition must be positive ($\sigma > 0$). Thus, from (27) and the fact (numerically demonstrated in Sec. V) that $dG/dh > 0$ if and only if $h > \bar{h}$, we conclude that h_σ and h_γ are greater than \bar{h} . This shows, as expected, that the fractal properties of the measure (D_q for $q > 0$) are determined by regions with greater than average stretching.

The fact that h_σ and h_γ are greater than \bar{h} is of significance for the case of the nonrandom maps. This is because, for nonrandom maps with integrable KAM regions, the form of $G(h)$ is modified, but only for $h < \bar{h}$. In particular, Horita *et al.*¹⁴ show that $G(h) = 0$ for $h < \bar{h}$, due to the weak stretching near KAM surfaces and the fact that orbits tend to stick near these surfaces once approached. Since the form of $G(h)$ for $h > \bar{h}$ is unchanged,¹⁴ our theory also applies to nonrandom maps with a mixture of KAM and chaotic regions. This is reasonable, since orbits which experience sticking to KAM regions will have lower than average h and do not contribute to the fractal properties of the measure considered here. Numerical results (not reported in this paper) have also been obtained for the nonrandom case and yield box counting dimensions D_q in agreement with Eqs. (27)–(30).

V. COMPARISON OF THEORY AND COMPUTATIONS

In this section, we obtain $G(h)$ numerically for the randomized standard map introduced in Sec. II, for the cases studied in Sec. III. We then explain the method used to obtain the dimension spectra shown as solid curves in Figs. 3–5. The comparison with box counting results is then discussed further.

The first step in applying the theory of Sec. IV is to obtain an approximate distribution of finite time Lyapunov exponents, $P(h, n)$, for the chaotic flow after long times. To obtain this distribution, we compute the average exponential growth rate of infinitesimal variations along trajectories of the flow, starting from a uniform grid of one million initial points in the square $0 < (x, y) < 2\pi$. Each initial point is assigned an infinitesimal variation

$$\delta \mathbf{x}(0) = (1, 0),$$

and the evolution of the variation is then computed by

$$\delta \mathbf{x}(n+1) = \mathbf{J}(\mathbf{x}_n, \theta_n) \cdot \delta \mathbf{x}(n),$$

where \mathbf{x}_n is the trajectory starting at \mathbf{x}_0 given by

$$\mathbf{x}_{n+1} = \mathbf{M}(\mathbf{x}_n, \theta_n).$$

\mathbf{M} is the randomized standard map of Eq. (13), with Jacobi matrix \mathbf{J} given by Eq. (14), and with forcing parameter $K = 0.5$. For times n of interest, the finite time Lyapunov exponents

$$h(n; \mathbf{x}_0) = \frac{1}{n} \ln \frac{|\delta \mathbf{x}(n)|}{|\delta \mathbf{x}(0)|}$$

are computed and binned to obtain a histogram of the number of initial conditions having values of h in any of 200 bins. Normalizing this histogram, so that the integral is unity, gives an approximation to the probability density $P(h, n)$. Figure 6 shows the typical behavior of $P(h, n)$ as n increases. Note the sharpening of the peak of P around $h = \bar{h}$ as n increases.

Taking the logarithm of the theoretical form (25) of $P(h, n)$ yields

$$G(h) = -\frac{1}{n} \ln P(h, n) + \frac{\ln n}{2n} + \frac{1}{2n} \ln \left(\frac{G''(h)}{2\pi} \right),$$

and for large n , the term containing $G''(h)$ can be neglected, leaving

$$G(h) \cong - (1/n) \ln P(h, n) + (\ln n)/2n. \quad (31)$$

Utilizing Eq. (31) and the $P(h, n)$ curves of Fig. 6, we obtain the graphs of $G(h)$ shown in Fig. 7. It appears that a limiting shape is being approached as $n \rightarrow \infty$, giving numerical evidence supporting Eq. (25) and the existence of $G(h)$ as a time invariant characteristic of the Lyapunov exponent distribution.

Utilizing the numerically determined $G(h)$, Eqs. (27)–(30) of Sec. IV can be applied to obtain the spectrum of dimensions of the gradient measure. First we rewrite the equations as follows. Using the condition (27), substitute $\sigma = G'(h_\sigma)$ and $\gamma = G'(h_\gamma)$ in Eq. (29), then rearrange and drop the subscript σ to obtain

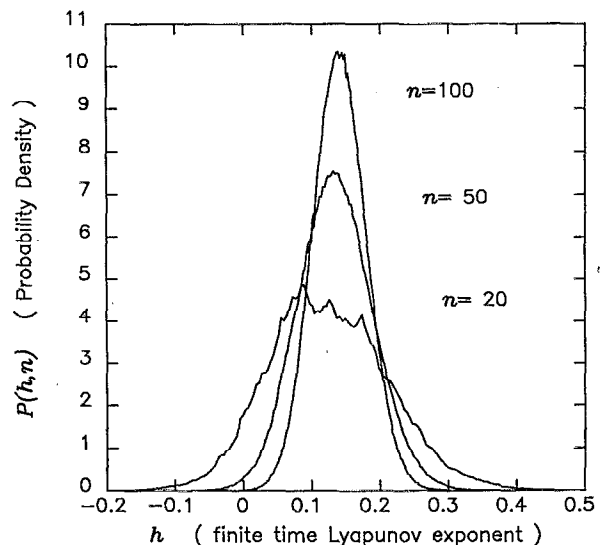


FIG. 6. The distribution, $P(h, n)$, of finite time Lyapunov exponents h , for iterates $n = 20, 50, 100$ of the randomized standard map [Eq. (13)], with $K = 0.5$.

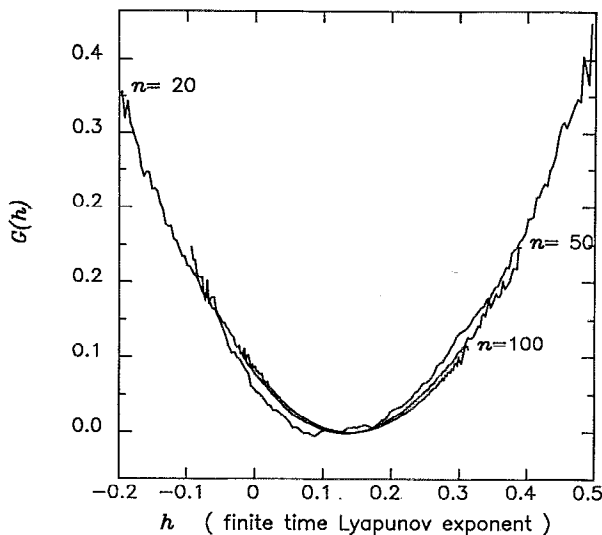


FIG. 7. The result of applying Eq. (31) to the curves of Fig. 6, yielding, for $n = 20, 50, 100$, graphs of $G(h)$, the function characterizing the Lyapunov exponent distribution [Eq. (25)].

$$q(h) = [G(h) - hG'(h)]/[G(h_\gamma) - h_\gamma G'(h_\gamma)], \quad (32)$$

a relation between the finite time Lyapunov exponents h and the dimension spectrum index q . Now, from Eq. (30), the dimension spectrum of μ_ϕ is given by

$$D_q = 2 - [\gamma q(h) - G'(h)]/[q(h) - 1]. \quad (33)$$

Since $G(\bar{h}) = 0$ and $G'(\bar{h}) = 0$, where \bar{h} is the asymptotic Lyapunov exponent, the equations give $q(\bar{h}) = 0$ and $D_0 = 2$, as expected.

To apply the preceding equations, we perform a linear least-squares fit of a third-order polynomial to the numerical $G(h)$ data. This eliminates the statistical fluctuations due to having a finite sample of initial conditions, and yields an analytic function which can be differentiated. Further, we note that the third-order polynomial is an excellent fit to the data, as shown in Fig. 8 for $n = 100$. To quantify the denominator of Eq. (32), we solve for the value h_γ which satisfies the condition (27)

$$\frac{dG}{dh}(h_\gamma) = \gamma,$$

where the derivative of G is obtained analytically from the polynomial fit. For $\gamma = 1$ we obtain $h_\gamma = 0.312$, and using this in Eq. (32) with the polynomial approximation of $G(h)$ then gives $q(h)$. The maximum value of $q(h)$ available from the numerical $G(h)$ in Fig. 8 is $q_{\max} \approx 1$, but it is possible to extrapolate slightly beyond that using the polynomial fit. Finally, the Lyapunov dimension spectrum of the gradient measure μ_ϕ is obtained from Eq. (33), and this result is shown as the solid curves in Figs. 3–5.

Examining the comparison in Fig. 4, we see that, when q is less than a certain critical value, the box counting dimension spectrum is greater than the dimension spectrum predicted from $G(h)$. This particular value of q we shall call the

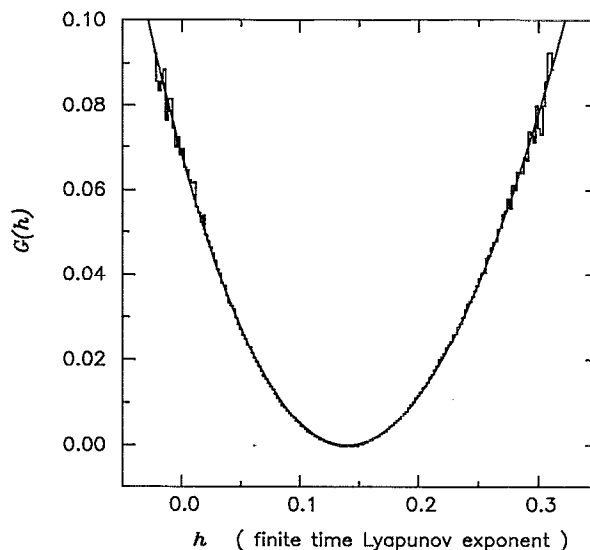


FIG. 8. The numerically obtained $G(h)$, for $n = 100$, is overplotted with a third-order polynomial fit: $G(h) \approx 0.07 - h + 3.88h^2 - 1.44h^3$. This polynomial fit is used to calculate the Lyapunov dimension spectrum, shown as the solid curves in Figs. 3–5.

crossover value, because, for q greater than the crossover value, the opposite situation occurs. Further, as the number of map iterations n increases, this crossover value moves from larger to smaller values of q , as inferred from Fig. 5. In the remainder of this section we explain the behavior of the box counting dimension spectrum relative to its theoretical prediction from $G(h)$, as a function of q and n .

When estimating the box counting dimension spectrum, an important question is: what minimum box size ϵ_{\min} should be used in the estimation? Using $G(h)$, we shall give a qualitative prediction of ϵ_{\min} as a function of (q, n) . Another way of looking at the definition (19) of dimension is that D_q determines the scaling exponent of the measure raised to the power q , as the box size ϵ goes to zero:

$$\sum_i \mu_i^q \sim \epsilon^{(q-1)D_q}. \quad (34)$$

In the preceding theory of the dimension spectrum [Eq. (33)], the spectrum index q and Lyapunov exponents h are indirectly related through the function $G(h)$ and Eq. (32). This leads to the interpretation that, the scaling exponent of the q moment of μ_ϕ is mainly due to those boxes having trajectories which yield Lyapunov exponents in the range $\Delta h_{\sigma(q)}$, given by Eq. (28), around the value $h_{\sigma(q)}$ determined by Eqs. (27) and (29). The fraction of trajectories contributing to this range $\Delta h_{\sigma(q)}$ about $h_{\sigma(q)}$ is approximately

$$P(h_{\sigma(q)}, n) \Delta h_{\sigma(q)} \sim \exp[-nG(h_{\sigma(q)})],$$

[obtained by multiplying Eqs. (25) and (28)]. If N_τ is the total number of trajectories, then $N_\tau \exp[-nG(h_{\sigma(q)})] \epsilon^d$ is approximately the number of trajectories in a box of size ϵ contributing to the q moment (34) of μ_ϕ , where d is the embedding dimension of the boxes (i.e., $d = 2$ when analyzing an image, $d = 1$ for a vertical cut). For adequate statis-

tics, the average number of contributing trajectories in a box must be much greater than one. Thus a bound on the minimum box size for observable scaling of the measure after n time steps is approximately

$$\epsilon_{\min} > \epsilon_G(q, n) = \{ \exp[nG(h_{\sigma(q)})] / N_T \}^{1/d}. \quad (35)$$

Note that ϵ_G is an increasing function of q and n . For box sizes smaller than ϵ_G , the q moment of μ_ϕ will tend to scale with an exponent corresponding to a lower fractal dimension, because of a lack of enough trajectories to accurately determine the measure in the boxes.

Another bound on the minimum box size arises from the fact that for finite time the measure is smooth on sufficiently small scale. To estimate the relevant scale for those trajectories with finite time Lyapunov exponent in the range $\Delta h_{\sigma(q)}$ about $h_{\sigma(q)}$, we note that the fluid elements following these trajectories have experienced a stretching of approximately $\exp(nh_{\sigma(q)})$, after n time steps. Since we are dealing with a conservative two-dimensional flow, those same fluid elements must have experienced a contraction by approximately $\exp(-nh_{\sigma(q)})$ in some other direction. Recall from the Introduction that it is the contraction of fluid elements which causes exponential growth of the gradient of the convected scalar field, and hence the scaling of the gradient measure with respect to box size. Therefore, the minimum box size for which scaling of the measure can be occurring after n time steps is approximately

$$\epsilon_{\min} > \epsilon_h(q, n) = \exp(-nh_{\sigma(q)}). \quad (36)$$

Note that ϵ_h is a decreasing function of q and n . For box sizes smaller than ϵ_h , the q moment of μ_ϕ will tend to scale with an exponent corresponding to a higher fractal dimension, because the measure is still smooth (i.e., two dimensional).

The estimation of the box counting dimension spectrum of μ_ϕ is affected by both the ϵ_h and ϵ_G bounds on the minimum box size for observable scaling. The dimension spectra shown in Figs. 4 and 5 are estimated by using the same range of box sizes, $\epsilon_{\min} \leq \epsilon \leq \epsilon_{\max}$, for all values of the spectrum index q and time n . Applying the preceding discussion of the relevance of ϵ_h and ϵ_G , the box counting dimension estimates will be greater than the theory [Eq. (33)] when the values of q and n cause $\epsilon_h(q, n) > \epsilon_{\min}$, and the box counting dimension estimates will be less than the theory when the values of q and n cause $\epsilon_G(q, n) > \epsilon_{\min}$. Figure 9 shows the combined quantity $\log_2 [\max\{\epsilon_h, \epsilon_G\}]$ versus spectrum index q , for $n = 30, 40, 50$ iterations, and $d = 1$ (one-dimensional boxes), corresponding to the box counting analysis results shown in Figs. 4 and 5. Each wedge shaped curve of Fig. 9 is composed of ϵ_h on the left-hand side of the minimum, and ϵ_G on the right side. The value of q where the box counting dimension estimate goes from being greater than to less than the predicted dimension is given approximately by the condition $\epsilon_h(q, n) = \epsilon_G(q, n)$ (the minima of the curves), and this crossover value decreases as n increases.

For fixed values of q and minimum box size ϵ_{\min} , the condition

$$\epsilon_{\min} > \max\{\epsilon_h(q, n), \epsilon_G(q, n)\}$$

estimates the values of n for which the scaling exponent of

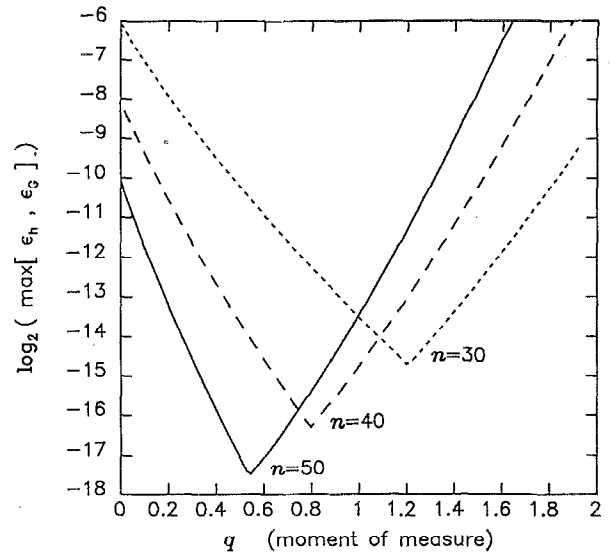


FIG. 9. Qualitative prediction of the minimum box size for the scaling range of the q moment of the gradient measure, when analyzing a one-dimensional cut of the measure (as in Figs. 4 and 5). Log base 2 of the approximate minimum box size is shown as function of q , at values of time $n = 30, 40, 50$. The curves are computed using the $G(h)$ of Fig. 8, as explained in text.

the q moment of μ_ϕ may be observed with box counting. Choosing $q = 1.0$ and $\epsilon_{\min} = 2^{-13}$ in Fig. 9 selects $30 \leq n \leq 50$ iterations as the approximate time range when the q moment of μ_ϕ will exhibit the theoretically predicted scaling exponent, for box sizes $\epsilon > \epsilon_{\min}$. This is the range of n where best agreement between the theory and box counting is found in Fig. 5, for $q = 1.0$. Similarly, for $q = 0.5$, Fig. 9 indicates that the theoretical scaling exponent will be estimated via box counting when $n > 40$, which is the case in Fig. 5. The loss of agreement for $n > 80$ in Fig. 5, is also qualitatively predicted by the scaling range cutoff $\epsilon_G(q, n)$, but is not shown in Fig. 9.

VI. CONCLUSION

The results of numerical simulations of a specific two-dimensional chaotic flow, demonstrate that the gradient of a passively convected scalar field tends to concentrate on a multifractal set, whose characteristics are determined by the chaotic properties of the flow. We believe that the flow which we investigate is representative of chaotic flows in general, and by including a random component in the shear velocity term it may represent some aspects of weakly turbulent flows. A measure is defined from the magnitude of the gradient of the scalar field, and, applying the technique of box counting, we have shown that the dimension spectrum of the gradient measure approaches a multifractal spectrum.

In addition, we verify a recent theory^{1,2} relating the dimension spectrum of the gradient measure to the nonuniform stretching (chaotic) properties of the flow. Passive convection (stretching) by the flow is characterized by computing the distribution of finite time Lyapunov exponents h , and a time invariant characteristic function $G(h)$ is then calculated² from the distribution of h . Using this character-

istic function $G(h)$, we can calculate the dimension spectrum of the gradient measure. The dimension spectrum, based on the Lyapunov exponent distribution, is found to be in reasonable agreement with the box counting dimension spectrum.

ACKNOWLEDGMENTS

This work was supported by the Office of Naval Research (Physics) and by the U.S. Department of Energy.

APPENDIX: CONVECTION OF CURVES AND SURFACES

Our problem of the evolution of $\nabla\phi$ is equivalent to looking at the evolution of an initially smooth line in two dimensions or a surface in three dimensions. The result that $|\nabla\phi|$ eventually concentrates on a fractal is equivalent to saying that the convected line or surface concentrates on a fractal (in a sense described below). In three dimensions, the evolution of a convected line is equivalent to the problem of the convection of a passive divergence-free vector field, which is also treated in Ref. 2 where the concentration of the vector on a fractal is related to the stretching properties of the flow (similar to the results summarized in Sec. IV for $\nabla\phi$). (The vector problem is of interest in the study of the fast kinematic dynamo.)

We now show the equivalences stated above, for the case of passive scalar gradients. Consider the evolution of a surface in three dimensions (or a line in two dimensions). Initially the surface is taken to be nonfractal and smooth (e.g., a spherical surface might be used initially). Now imagine that the surface is evolved for a long time, developing many folds and layers. We define a measure μ_i for a cube i , as in Sec. III, by saying that μ_i is the fraction of the area of the evolved surface which lies in the i th cube (box in two dimensions). Note that, for sufficiently large time, the surface will pass through the box many times. The dimension spectrum D_q is then as given in Eq. (19).

Now consider the evolution of $\nabla\phi$, where we take the initial scalar distribution $\phi(\mathbf{x},0)$ to be a constant ϕ_1 in some region and a different constant ϕ_2 in the complement of this region. Further we take the initial surface separating these regions to be smooth and nonfractal. We evolve ϕ for this initial condition under Eq. (2) and compute μ_i for each cube as defined by (9) for $\gamma = 1$. Noting that ϕ is constant following an orbit, by Eqs. (2) and (3), we see that the surface separating the region with $\phi = \phi_1$ from the region with $\phi = \phi_2$, is convected with the flow. Application of the definition of μ_ϕ given in Eq. (9), for $\gamma = 1$, shows that the measure μ_i of a cube is just the fraction of the evolved surface area in the cube. Hence, the two problems are equivalent.

- ¹ E. Ott and T. M. Antonsen, Phys. Rev. Lett. **61**, 2839 (1988).
- ² E. Ott and T. M. Antonsen, Phys. Rev. A **38**, 3660 (1989).
- ³ Some recent papers on the convection of passive scalars in chaotic flows: H. Aref, J. Fluid Mech. **143**, 1 (1984); T. Dombre, U. Frisch, J. M. Greene, M. Hénon, A. Mehr, and A. M. Soward, *ibid.* **167**, 353 (1986); D. V. Khakhar, H. Rising, and J. M. Ottino, *ibid.* **172**, 419 (1986); N. R. A. Hoffman and D. P. McKenzie, Geophys. J. R. Astron. Soc. **82**, 163 (1985); J. Chaiken, C. K. Chu, M. Tabor, and Q. M. Tran, Phys. Fluids **30**, 687 (1987); S. W. Jones and H. Aref, *ibid.* **31**, 485 (1988); T. H. Solomon and J. P. Gollub, *ibid.* **31**, 1372 (1988); J. M. Ottino, *The Kinematics of Mixing: Stretching, Chaos, and Transport* (Cambridge U.P., Cambridge, 1989).
- ⁴ P. Grassberger, R. Badii, and A. Politi, J. Stat. Phys. **51**, 135 (1988); R. Badii and A. Politi, Phys. Rev. A **35**, 1288 (1987).
- ⁵ R. R. Prasad, C. Meneveau, and K. R. Sreenivasan, Phys. Rev. Lett. **61**, 74 (1988); R. Ramashankar and J. Gollub, submitted to Phys. Fluids A.
- ⁶ A. Rényi, *Probability Theory* (North-Holland, Amsterdam, 1970).
- ⁷ P. Grassberger, Phys. Lett. A **97**, 227 (1983).
- ⁸ H. G. E. Hentschel and I. Procaccia, Physica D **8**, 435 (1983).
- ⁹ J. D. Farmer, E. Ott, and J. A. Yorke, Physica D **7**, 153 (1983).
- ¹⁰ P. Grassberger, Phys. Lett. A **107**, 101 (1983).
- ¹¹ T. C. Halsey, M. J. Jensen, L. P. Kadanoff, I. Procaccia, and B. I. Shraiman, Phys. Rev. A **33**, 1141 (1986).
- ¹² T. M. Morita, H. Hata, H. Mori, T. Horita, and K. Tomita, Prog. Theor. Phys. **78**, 511 (1987).
- ¹³ M. A. Sepúlveda, R. Badii, and E. Pollak, Phys. Rev. Lett. **63**, 1226 (1989).
- ¹⁴ T. Horita, H. Hata, R. Ishizaki, and H. Mori, Prog. Theor. Phys. **83**, 1065 (1990).